



1st International Conference on the Material Point Method, MPM 2017

Adhesive contact algorithm for MPM and its application to the simulation of cone penetration in clay

Francesca Ceccato^{a,*}, Lars Beuth^b, Paolo Simonini^a

^a DICEA – University of Padua, via Ognissanti 39, 35129 Padua, Italy

^b Deltares, Delft, The Netherlands

Abstract

Contact between bodies is one of the most challenging problems to solve, especially when combined with large deformations. For MPM, several methods have been developed to simulate frictional contact, i.e. shear stress is proportional to the normal stress via a friction coefficient; however, for cohesive soils under undrained conditions the interface shear stress is more likely a function of the undrained shear strength and independent of the normal stress (adhesive contact). This paper presents the extension of one of the most widely used contact algorithms in MPM for adhesive contact. This enhanced formulation is validated with a sliding block benchmark and applied to the simulation of cone penetration testing (CPT) in clay. CPT is an in situ test commonly used in geoenvironmental engineering to determine the subsoil's stratigraphy and to estimate soil parameters. It is shown that the adhesion at the cone-soil interface affects significantly the measured cone resistance. Numerical results are compared with available analytical and experimental studies, showing the effectiveness of the proposed method to describe undrained penetration in clay.

© 2016 The Authors. Published by Elsevier Ltd.

Peer-review under responsibility of the organizing committee of the 1st International Conference on the Material Point Method.

Keywords: contact algorithm; CPT; adhesive contact.

1. Introduction

Contact between a structure and soil is widely encountered in geotechnical applications such as penetration problems, impact of landslides on defense structures, and stability of retaining structures. Modelling of such contact is a persistent challenge in various numerical methods, especially when the contact involves large displacements and

* Corresponding author.

E-mail address: francesca.ceccato@dicea.unipd.it

failure within the adjacent soil. With the Material Point Method (MPM) there are several possibilities to take into account the soil-structure interaction such as the use of interface elements [1], level-set based contact algorithms [2], or multi-velocity field formulations [3–5]. In this study, the contact algorithm proposed by Bardenhagen et al. [5] is considered. The advantage of this algorithm is that it automatically detects the contact surface and does not require any special interface elements. It proved to be efficient in modeling interaction between solid bodies as well as shearing in granular materials [6,7].

The original formulation considers only the Coulomb friction model, i.e. the maximum shear stress along the interface is proportional to the normal stress. For cohesive soils under undrained conditions, this mechanism is unrealistic. Indeed, the interface shear stress is more likely a function of the undrained shear strength and independent of the normal stress, thus an adhesive contact law seems more appropriate.

In this study, the original frictional algorithm is extended for adhesive contact as presented in Section 2. This enhanced formulation has been implemented in Anura3D (www.anura3D.eu), validated and applied to the simulation of the cone penetration test (CPT) in clay under undrained conditions. The effect of adhesion at the soil-cone interface on the measured tip resistance is investigated and compared with other numerical results as well as experimental evidences.

2. The adhesive contact algorithm

In MPM, the contact conditions are applied via the background grid and the contact problems can be completely described by the nodal variables. The applied approach is based on a multi-velocity field formulation and can be considered as a predictor-corrector scheme. The nodal velocities are predicted from the solutions of each body considered separately and then corrected using the nodal velocities of the combined set of bodies according to the contact law. Figure 1 shows a flow chart of the procedure. For further details the reader is referred to [5,8]. In the following, the focus lies on the derivation of the expression for the corrected nodal velocities including both friction and adhesion.

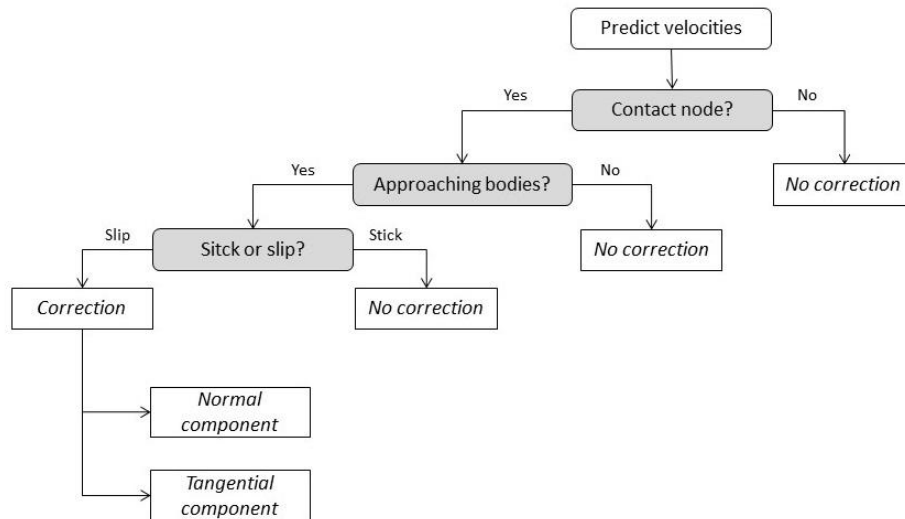


Fig. 1. Flow chart of the contact algorithm [9].

Let us consider two bodies A and B in sliding contact at time t . The single body velocities $\mathbf{v}_{k,A}$, $\mathbf{v}_{k,B}$ and the velocity of the combined system $\mathbf{v}_{k,S}$ are computed by solving the respective equations of motion. For a contact node k , the predicted single body velocity $\mathbf{v}_{k,A}$ of body A is corrected from:

$$\tilde{\mathbf{v}}_{k,A} = \mathbf{v}_{k,A} + \mathbf{c}_{k,norm} + \mathbf{c}_{k,tan} \quad (1)$$

where $\mathbf{c}_{k,norm}$ is the correction for the normal component, preventing interpenetration, and $\mathbf{c}_{k,tan}$ is the correction for the tangential component.

This correction is equivalent to applying the following contact forces:

$$\mathbf{f}_{k,norm} = \frac{m_{k,A}}{\Delta t} \mathbf{c}_{k,norm} \quad (2)$$

$$\mathbf{f}_{k,tan} = \frac{m_{k,A}}{\Delta t} \mathbf{c}_{k,tan} \quad (3)$$

where $m_{k,A}$ is the nodal mass and Δt the time step size. The correction of the normal component is calculated in such a way that the normal component of the new single body velocity and the normal component of the combined bodies $\mathbf{v}_{k,s}$ are equal, i.e.:

$$\mathbf{c}_{k,norm} = -[(\mathbf{v}_{k,A} - \mathbf{v}_{k,S}) \cdot \mathbf{n}_{k,A}] \mathbf{n}_{k,A} \quad (4)$$

where $\mathbf{n}_{k,A}$ is the unit outward normal vector of body A at contact node k . The maximum contact force depends on the friction coefficient μ and the adhesion factor a :

$$\mathbf{f}_{k,tan,max} = (\mu |\mathbf{f}_{k,norm}| + a A_k) \mathbf{t}_k \quad (5)$$

where A_k is the surface area associated with node k and \mathbf{t}_k is the tangential unit vector. Combining Equations 1 to 5, the corrected velocity takes the following expression:

$$\tilde{\mathbf{v}}_{k,A} = \mathbf{v}_{k,A} - [(\mathbf{v}_{k,A} - \mathbf{v}_{k,S}) \cdot \mathbf{n}_{k,A}] \mathbf{n}_{k,A} + [(\mathbf{v}_{k,A} - \mathbf{v}_{k,S}) \cdot \mathbf{n}_{k,A}] \mu \mathbf{t}_k - \frac{a A_k \Delta t}{m_{k,A}} \mathbf{t}_k \quad (6)$$

Note that the second term on the right-hand-side is the correction of the normal component to avoid interpenetration, the third and the fourth terms are the correction of the tangential component due to friction and adhesion respectively. The same relationship can be derived for body B.

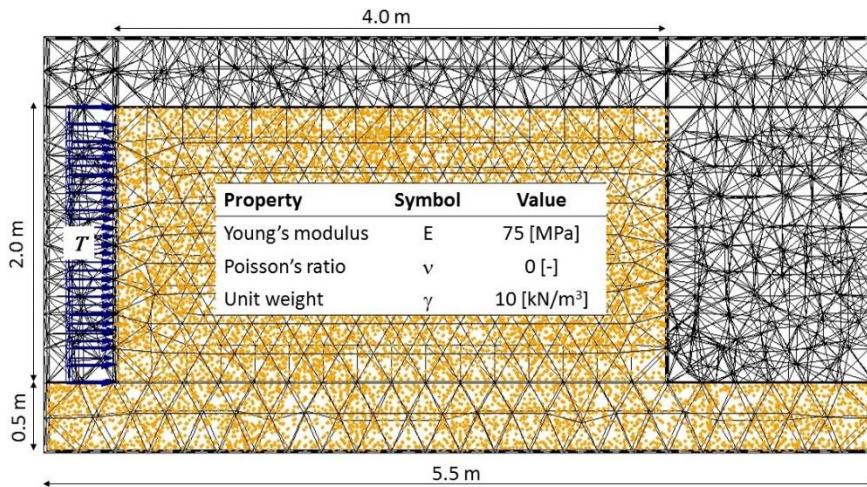


Fig. 2. Geometry, discretization and material properties of the sliding block benchmark.

3. Validation of the adhesive contact

The implemented contact algorithm is validated with a benchmark problem consisting in two sliding blocks. The upper one has dimensions $2.0 \times 4.0 \times 0.5 \text{ m}^3$. It is pushed by a horizontal force T linearly increasing in time with a rate of 1 kN/s . The lower block has dimensions $0.5 \times 5.5 \times 0.5 \text{ m}^3$. The two blocks share a contact surface of area of 2 m^2 (Fig. 2). At the boundaries, displacements are constrained in normal direction. The contact surface is characterized by an adhesion $a = 10 \text{ kPa}$, which gives a maximum tangential contact force $F_{tan,max} = 20 \text{ kN}$.

As expected, the kinetic energy of the system remains nearly zero while $T < F_{tan,max}$; beyond this value it increases suddenly, meaning that the block is sliding (Fig. 3a).

Figure 3b plots the tangential (F_{tan}) and the normal (F_{norm}) component of the contact force over the applied external load. The contact forces show some oscillations that increase when the block starts sliding. They can be reduced by refining the mesh or decreasing the time step size. The average values agree with theoretical expectations proving the validity of the implemented contact algorithm. As expected, the normal force is constant and equal to the block weight, while the tangential force increases linearly with T up to 20 kN and they remains constant.

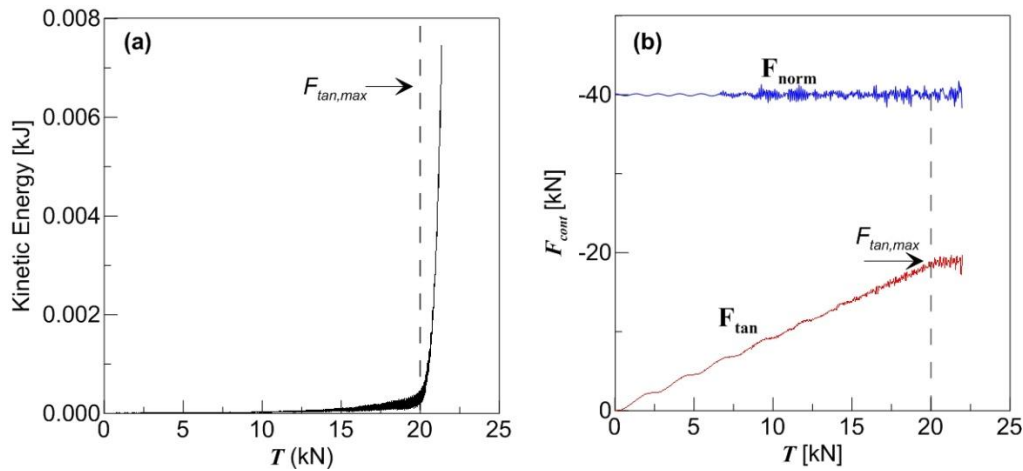


Fig. 3. (a) Kinetic energy of the system of sliding block, (b) Normal and tangential contact forces on the sliding block.

4. Application to CPT simulation

The cone penetration test is a widely used in situ soil testing technique applied to identify the subsoil profile and to estimate soil properties. It consists of pushing a steel cone with a measuring device attached to its tip into the ground with a constant velocity of 2 cm/s . The derived measurements of tip resistance, q_c , and sleeve friction, f_s , are correlated to soil characteristics [10].

In saturated fine-grained soils, the cone resistance may be interpreted as a measure of undrained shear strength. Conventionally, the undrained shear strength (s_u) is derived by dividing the net cone resistance by a cone factor N_c :

$$s_u = \frac{q_c - \sigma_{v0}}{N_c} \quad (7)$$

where σ_{v0} is the local vertical stress. The cone factor depends on the cone roughness, the in situ stress state and the rigidity index $I_r = G/s_u$ where G is the shear modulus [11]. In the following, the numerical model is described and the effect of adhesion on the cone factor is discussed. The non-dimensional parameter $\alpha_c = a/s_u$ is introduced to quantify the cone roughness.

4.1. Setup of the numerical model

Taking advantage of the rotational symmetry of the cone penetration problem, only a 20° slice is considered with the used 3D code. The cone is slightly rounded in order to circumvent numerical problems induced by a discontinuous edge at the base of the cone. Apart from this modification, the dimensions of the penetrometer correspond to those of a standard penetrometer: the apex angle is 60° and the cone diameter D is 0.036 m.

The size and the refinement of the mesh have been determined through preliminary calculations as a compromise between computational cost and accuracy (Fig. 4a) [12]. It counts 13221 tetrahedral elements and 105634 material points are located in the initially active elements. 20 MP are initially placed inside each element near and below the tip, while 10 or 4 MP fill those elements further away from the cone. Displacements are constrained in normal direction at the lateral mesh surfaces, while the bottom of the mesh is fully fixed.

The penetrometer moves downward by a prescribed velocity of 2 cm/s applied at the nodes of the structure, which therefore behaves as a rigid body. In order to keep the fine mesh always around the cone, the so-called moving mesh procedure is adopted [9,13,14]. It consists in adjusting the part of the mesh adjacent to the penetrometer (Fig. 4b) to the movement of the cone after each time step, ensuring that the penetrometer surface coincides with element boundaries. The elements of this zone keep the same shape throughout the computation, while elements in a compressed zone below the penetrometer reduce their vertical length. The adopted discretization of the compressed zone guarantees a reasonable aspect ratio ($0.3 < a < 3$) of the elements throughout the analysis. With this approach the unit normal vectors of Equation 6 at nodes on the penetrometer surface do not change and hence a possible inaccuracy related to recomputing them is eliminated.

The undrained behavior of clay is described with an elastic perfectly plastic model with Tresca failure criteria. The undrained shear strength is 20 kPa and the Young's modulus is 6000 kPa. Soil incompressibility is simulated by assuming a Poisson's ratio of 0.49. The problem is characterized by a rigidity index $I_r = 100$. For simplicity, initial stresses are set to zero.

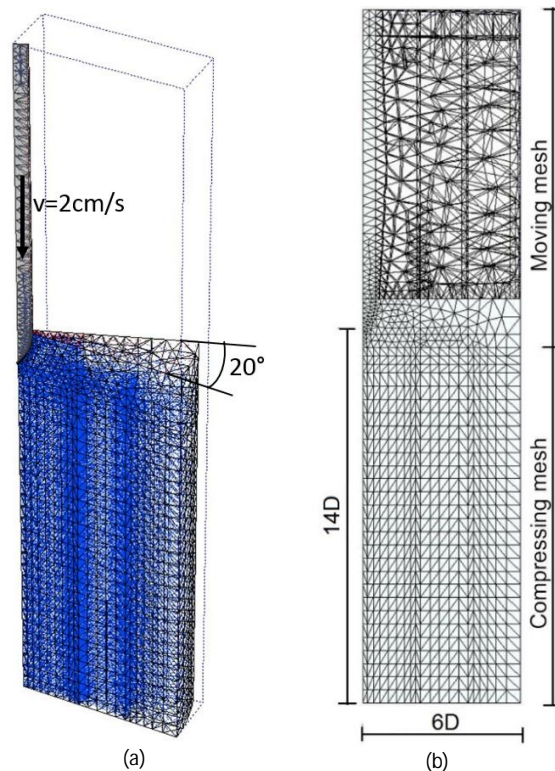


Fig. 4. Geometry and discretization of the CPT problem; (a) material point discretization; (b) FE discretization. ($D = 0.036$ m)

4.2. Results

Figure 5 shows the tip stress as a function of the normalized penetration for different cone roughness. The steady state solution, which corresponds to the tip resistance, is reached after about 7D penetration, independently of α_c .

The computed cone factor increases from 10.2 in case of smooth cone ($\alpha_c=0$) to 15.8 in case of a very rough cone ($\alpha_c=1$). According to [15], α_c ranges between 0.25 and 0.5 for steel in contact with clay. For this range of values, the MPM simulations give N_c between 12 and 14. This is in excellent agreement with the experimental data based on calibration chamber tests by [16] in which a cone factor $N_c = 13$ was found for a rigidity index $I_r = 100$.

Figure 6 compares cone factors obtained with other numerical methods for 3 values of α_c and similar rigidity index and stress state. Previous analyses of CPT in clay adopted the Arbitrary Lagrangian-Eulerian method [17,18], the implicit quasi-static MPM [13] or the Coupled Eulerian-Lagrangian (CEL) method [19]. These studies applied the Tresca constitutive model for clay and simulated the soil-cone interaction using interface elements. For values of α_c typical of this problem previous studies appear to underestimate the cone factor observed experimentally. For smooth cone, the result of this study agrees with results of other numerical studies, but slightly higher values of N_c are obtained for α_c equal to 0.5 and 1. This suggests that the differences may be mainly due to the technique adopted to simulate the soil-cone interaction, which is thus of primary importance in soil-penetration problems. Further investigations are necessary to identify in more details the source of these discrepancies.

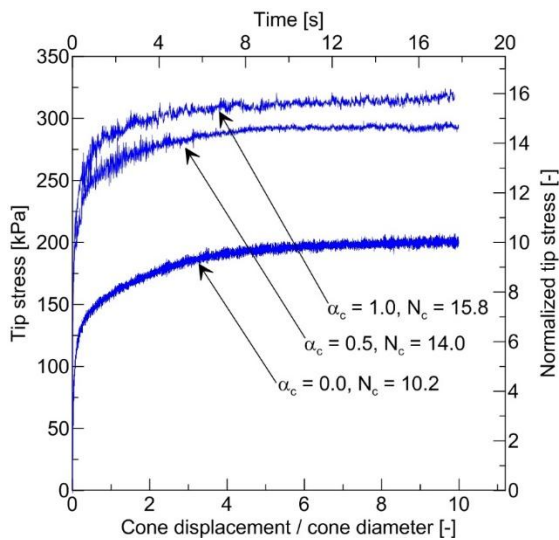


Fig. 5. Tip stress over normalized displacement.

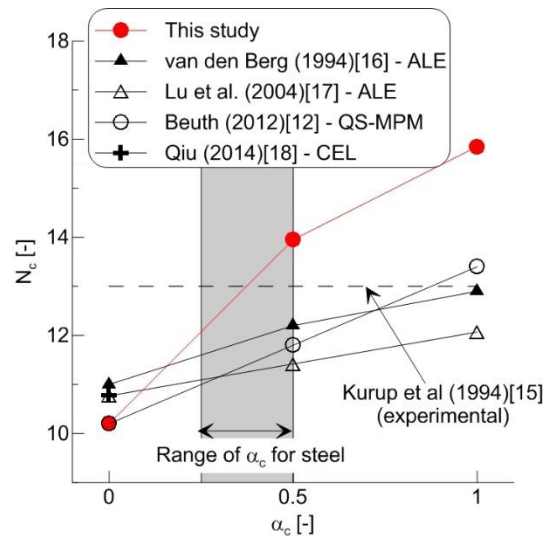


Figure 6 Cone factors obtained with different methods.

5. Conclusions

This paper presents an extension of the frictional contact algorithm originally proposed by [5] to include adhesion. The algorithm was implemented in the MPM code Anura3D and validated with a sliding-block benchmark. The extended contact algorithm appears applicable to a wide range of problems of soil-structure interaction. In this paper, it is applied to the simulation of CPT in clay analyzing the effect of cone roughness on the cone factor. For typical values of cone roughness, numerical results are in good agreement with experimental evidences and with previous numerical studies thus proving the validity of the method.

Acknowledgments

The authors thank Dr. Eng. Issam Al-Kafaji, former Deltares employee and Prof. Pieter A. Vermeer for their significant contributions to this study.

References

- [1] P.A. Vermeer, Y. Yuan, L. Beuth, P. Bonnier, Application of interface elements with the Material Point Method, in: Proc. 18th Int. Conf. Comput. Methods Mech., Zielona Gora, Poland, 2009: pp. 477–478.
- [2] L. Lim, On the application of the material point method for offshore foundations, in: M. Hicks, Brinkgreve, A. Rohe (Eds.), Numer. Methods Geotech. Eng., Taylor and Francis group, 2014: pp. 253–258.
<https://books.google.it/books?hl=it&lr=&id=31DvBQAAQBAJ&oi=fnd&pg=PA253&dq=On+the+application+of+the+material+point+method+for+offshore+foundations&ots=BoK8bun0Mq&sig=791ZXtwnCW1Jr2kTGKq4RAArW0A> (accessed May 4, 2015).
- [3] J. Ma, D. Wang, M. Randolph, A new contact algorithm in the material point method for geotechnical simulations, Int. J. Numer. Anal. Methods Geomech. (2014) 1197–1210. doi:10.1002/nag.
- [4] P. Huang, X. Zhang, Contact algorithms for the material point method in impact and penetration simulation, Int. J. Numer. Methods Eng. (2011) 498–517. doi:10.1002/nme.
- [5] S.G. Bardenhagen, J.E. Guilkey, K.M. Roessig, J.U. Brackbill, W.M. Witzel, J.C. Foster, An improved contact algorithm for the material point method and application to stress propagation in granular material, C. - Comput. Model. Eng. Sci. 2 (2001) 509–522.
- [6] C.J. Coetzee, P.A. Vermeer, A.H. Basson, The modelling of anchors using the material point method, Int. J. Numer. Anal. Methods Geomech. 29 (2005) 879–895. doi:10.1002/nag.439.
- [7] H.W. Zhang, K.P. Wang, Z. Chen, Material point method for dynamic analysis of saturated porous media under external contact/impact of solid bodies, Comput. Methods Appl. Mech. Eng. 198 (2009) 1456–1472. doi:10.1016/j.cma.2008.12.006.
- [8] I.K.J. Al-Kafaji, Formulation of a Dynamic Material Point Method (MPM) for Geomechanical Problems, Ph.D. thesis, University of Stuttgart, Germany, 2013. <http://elib.uni-stuttgart.de/opus/volltexte/2013/8549/>.
- [9] F. Ceccato, L. Beuth, P.A. Vermeer, P. Simonini, Two-phase Material Point Method applied to the study of cone penetration, Comput. Geotech. (2016). doi:10.1016/j.compgeo.2016.03.003.
- [10] T. Lunne, P. Robertson, J. Powell, Cone Penetration Testing in Geotechnical practice, EF Spon/Routledge Publ., New York, 1997.
http://books.google.com/books?id=ofbnE1xMI_kC&pgis=1
<http://www.ejge.com/iGEM/Books/br-lunne.htm>.
- [11] H. Yu, J. Mitchell, Analysis of cone resistance: review of methods, J. Geotech. Geoenvironmental Eng. 124 (1998) 140–149.
[http://ascelibrary.org/doi/abs/10.1061/\(ASCE\)1090-0241\(1998\)124:2\(140\)](http://ascelibrary.org/doi/abs/10.1061/(ASCE)1090-0241(1998)124:2(140)) (accessed September 27, 2013).
- [12] F. Ceccato, Study of large deformation geomechanical problems with the Material Point Method, Ph.D. thesis, University of Padua, Italy, 2014. http://paduaresearch.cab.unipd.it/7478/1/Ceccato_Francesca_tesi.pdf.
- [13] L. Beuth, Formulation and Application of a Quasi-Static Material Point Method, Ph.D. thesis, University of Stuttgart, Germany, 2012.
<http://elib.uni-stuttgart.de/opus/volltexte/2012/7364/>.
- [14] N.T.V. Phuong, A.F. van Tol, A.S.K. Elkadi, A. Rohe, Numerical investigation of pile installation effects in sand using material point method, Comput. Geotech. 73 (2016) 58–71. doi:10.1016/j.compgeo.2015.11.012.
- [15] J. Potyondy, Skin friction between various soils and construction materials, Geotechnique. 11 (1961) 339–353.
<http://www.icevirtuallibrary.com/content/article/10.1680/geot.1961.11.4.339> (accessed December 12, 2014).
- [16] P. Kurup, G. Voyiadjis, M. Tumay, Calibration chamber studies of piezocone test in cohesive soils, J. Geotech. Eng. 120 (1994) 81–107.
[http://ascelibrary.org/doi/abs/10.1061/\(ASCE\)0733-9410\(1994\)120:1\(81\)](http://ascelibrary.org/doi/abs/10.1061/(ASCE)0733-9410(1994)120:1(81)) (accessed December 12, 2014).
- [17] P. van den Berg, Analysis of soil penetration, Ph.D. thesis, TU Delft, 1994.
- [18] Q. Lu, Y. Hu, M.F. Randolph, I.C. Bugarski, A numerical study of cone penetration in clay, Géotechnique. 54 (2004) 257–267.
doi:10.1680/geot.2004.54.4.257.
- [19] G. Qiu, Numerical analysis of penetration tests in soils, in: J. Grabe (Ed.), Ports Contain. Ships Futur. Gener., Hamburg, Germany, 2014: pp. 183–196.